• Basic Research •

Development of a novel ultraviolet-polymerized hydrogel as an orbital implant

Fu-Bao Zhang[1], Yi-Li Chang[2], Xu-Zhang Tao[3], Feng Liu[4], Chun-Mei Liu[5], Hai-Jian Hu[6], Nian Fang[7]

[1]School of Information Management, Jiangxi University of Finance and Economics; Department of Stomatology, The Third Affiliated Hospital of Nanchang University, Nanchang 330008, Jiangxi Province, China
[2]Department of Ophthalmology, Affiliated Eye Hospital of Nanchang University, Nanchang 330006, Jiangxi Province, China
[3]Department of Nuclear Medicine, The Third Affiliated Hospital of Nanchang University, Nanchang 330008, Jiangxi Province, China
[4]School of Chemistry and Chemical Engineering, Nanchang University, Nanchang 330031, Jiangxi Province, China
[5]Medical Graduate School of Nanchang University, Nanchang 330006, Jiangxi Province, China
[6]Department of Ophthalmology, The Second Affiliated Hospital of Nanchang University, Nanchang 330006, Jiangxi Province, China
[7]Department of Gastroenterology, The Third Affiliated Hospital of Nanchang University, Nanchang 330008, Jiangxi Province, China
Co-first Authors: Fu-Bao Zhang and Yi-Li Chang
Correspondence to: Nian Fang. Department of Gastroenterology, The Third Affiliated Hospital of Nanchang University, Nanchang 330008, Jiangxi Province, China. fnian3893@126.com
Received: 2025-07-29 Accepted: 2026-02-04

Abstract

● **AIM:** To prepare ultraviolet (UV)-crosslinked hydrogel serving as a biocompatible orbital filler, and to explore its biological characteristics as well as its efficacy in expanding orbital soft tissue.

● **METHODS:** A novel medical hydrogel was fabricated *via* UV-induced photopolymerization. Its biosafety was assessed through cytotoxicity test, hemolysis assay and cell apoptosis detection. *In vivo* imaging examinations were conducted to observe the regulatory effect of the prepared hydrogel on orbital tissue development.

● **RESULTS:** The target hydrogel was successfully synthesized by photopolymerization, which possessed typical three-dimensional network structure, favorable hydrophilicity, appropriate swelling behavior and satisfactory mechanical performance. Biosafety evaluations confirmed its good biocompatibility with no obvious cytotoxicity, hemolytic reaction or abnormal cell apoptosis observed. *In vivo* implantation in juvenile rabbit orbits caused no evident pathological changes in major visceral organs. Imaging findings verified that the hydrogel could promote orbital tissue development, exerting reliable orbital expansion effects with favorable biological safety.

● **CONCLUSION:** The UV-crosslinked medical hydrogel prepared in this study has stable physicochemical properties and excellent biocompatibility. It can effectively expand orbital tissue.

● **KEYWORDS:** hydrogel; biocompatibility; orbital implant; rabbits

DOI:10.18240/ijo.2026.07.06

Citation: Zhang FB, Chang YL, Tao XZ, Liu F, Liu CM, Hu HJ, Fang N. Development of a novel ultraviolet-polymerized hydrogel as an orbital implant. *Int J Ophthalmol* 2026;19(7):1268-1277

INTRODUCTION

It is widely accepted that childhood enucleation causes orbital bone dysplasia and facial asymmetry[1-2]. Under normal conditions, human orbital bones and skull will develop in a certain proportion to meet and adapt to the exponential increase in eyeball volume during development. The normal orbital bone structure has left-right symmetry during growth and maturity, and the period before 1 year of age is the critical peak period for human orbital growth and development[3-5]. Small eyeball volume caused by congenital developmental abnormalities or eyeball loss caused by trauma, intraocular tumors and other diseases can lead to insufficient orbital content, a drop in orbital pressure, and reduced orbital stimulation, resulting in orbital and facial bone development delays and destruction of the symmetry of the double orbital structure, especially for children with unilateral disease[6]. Clinically, an orbital filler is usually implanted immediately after enucleation to stimulate the growth of the orbital bone

in a timely manner, restore the orbital volume, improve the appearance of the child, and prevent certain syndromes after enucleation[7-9].

Conventional methods to promote orbital bone development involve the use of rigid fillers with fixed orbital implant sizes. The most commonly used materials are hydroxyapatite balls with different diameters. Hydroxyapatite balls bearing porous structures in the center are advantageous to support vascular growth, reduce infection, displacement, and prolapse. However, placement of a hydroxyapatite ball may cause considerable surgical trauma and intricate complications and request additional implant replacement[10-12]. Moreover, there could be orbital growth retardation in treated children associated with orbital implantation of hydroxyapatite during earlier years after surgery[13].

Hydrogels, which can promote cell migration and growth, induce stem cell differentiation, and expand soft tissue, are widely applied in tissue engineering and regenerative medicine[14-19], offering promising potential as a biocompatible filler to expand the facial surface, particularly the orbital tissue. The swelling process of hydrogels generally has two stages: in the first stage, the solvent quickly enters the hydrogel to form a solvation layer, which is usually accompanied by a decrease in volume and heat release as the increase in the volume of the hydrogel itself is smaller than that of the liquid entering the hydrogel; the second stage is continuous solvent penetration that leads to an increase in hydrogel volume[20-22]. The three-dimensional polymer network structure and excellent water sealing ability enable hydrogels to form a stable spatial structure to provide mechanical support[23-26]. Hydrogels exhibit tailorable mechanical properties and high elasticity, achieved by controlling their degree of polymerization and crosslinking network structure[27]. The properties of polymer-based hydrogels could be tailored by selecting specific hydrophilic polymers or adopting *in-situ* controlled polymerization of hydrophilic monomers *via* radical polymerization or step condensation polymerization followed by appropriate crosslinking techniques[28-30]. Photopolymerization is an important and frequently employed method to prepare polymerized hydrogel due to its merits like precise and controllable polymerization in a three-dimensional manner, *in-situ* crosslinking, small energy demand, and easy and controllable operating procedures[31-35].

Here in this study, we developed an ultraviolet (UV)-polymerized hydrogel as a biocompatible filler to expand the facial surface, particularly the orbital tissue. The photopolymerized hydrogel system is composed of a UV initiator [2-hydroxy-4'-(2-hydroxyethoxy)-2-methylphenylacetone (Irgacure 2959)], hydrophilic monomer [methyl methacrylate (MMA) and N-vinylpyrrolidone (NVP)], the crosslinking agent [allyl methacrylate (AMA) and ethylene glycol dimethacrylate (EDGM)].

MATERIALS AND METHODS

Ethical Approval All animal protocols were approved by the Ethical Review Committee of the Affiliated Eye Hospital of Nanchang University (protocol number: YLP20221217). This study adhered to ARRIVE guidelines.

Materials Fetal bovine serum was obtained from Viva Cell Bioscience Co., Ltd. (Shanghai, China). RPMI 1640 cell culture medium was obtained from Solarbio Science & Technology Co., Ltd. (Beijing, China). The cell counting kit-8 (CCK-8) and Annexin V-PE/7-AAD Apoptosis Detection Kit were obtained from Yeasen Biotechnology Co., Ltd. (Shanghai, China). Other reagents and solvents were of analytical grade and used directly without further treatment.

Preparation of UV Polymerized Hydrogel Using the photoinitiator Irgacure 2959, monomer MMA, and NVP, crosslinking agent AMA and EDGM, the hydrogel was synthesized according to the ensuing procedure. MMA and NVP in mass ratio of 1:2.5, 0.1% AMA and 0.01% EDGM in mass ratio of monomer was mixed evenly under stirring, followed by adding 0.5% wt Irgacure 2959 in ethanol. Photopolymerization is initiated with an LED UV lamp at a wavelength of 365 nm and an intensity of 190 mW/cm^2 to prepare the crosslinked hydrogel.

Characterization of the UV-Polymerized Hydrogel The hydrogel synthesized by polymerization under UV irradiation was dry, which was submerged into 0.9% sodium chloride solution to absorb water and swell. The fully swelled hydrogel was placed into a vacuum freeze dryer to remove the internal water. The dry hydrogel, swollen hydrogel, and freeze-dried hydrogel were observed by the naked eye and under an optical microscope. The characteristics of the hydrogel in the three states were recorded, and the photos were taken. Additionally, the dry hydrogel and the freeze-dried hydrogel were placed in a vacuum drying oven for 1h to remove volatile impurities, after which each sample was placed in the observation area of the scanning electron microscope and images were taken at different magnifications.

Contact Angle Measurements The UV-polymerized dry hydrogel was fixed on the sample table, and the Theta Flex optical contact angle meter program was used after the level was adjusted. The sampler above the stage was fixed, and the camera focus was adjusted to acquire clear images. Deionized water was poured into the sampler and one drop was added to the surface of the dry hydrogel. Photographs were taken the moment the drop of water was added to measure the contact angle.

Determination of the Swelling Rate The swelling rate of the hydrogel was determined by measuring weight increase after soaking in water. First, and the dry hydrogel was weighed

on an electronic balance. A closed wide mouth glass reagent bottle filled with 0.9% sodium chloride was placed into a 37°C constant temperature water bath, and then the dry hydrogel was placed in the glass reagent bottle, ensuring that the sodium chloride solution could completely submerge the hydrogel. The weight of the hydrogel was measured once every hour in the one-day group and once a day for 4wk in the 4-week group. The weight of the hydrogel was recorded at each time point, and the swelling rate (SRt) was calculated at each time point as follows: SRt=(Wt-Wd)/Wd×100%, where *SRt* is the hydrogel swelling rate at time *t* (%), *Wt* is the hydrogel weight at time *t*, and *Wd* is the weight of the dry hydrogel. Additionally, the hydrogel swelling curve was plotted using *SRt vs t*.

Determination of the Anti-Compression Strength The hydrogel was placed in the center of the compression platform for measurement, and its diameter was measured. A universal mechanical testing machine (INSTRON 2343) was used for the measurements. The test method was set as compression, the speed of the loading beam was 10 mm/min, and the pound force sensor was set to 1.0 kN. The force measured by the pound force sensor gradually increased and then suddenly decreased when the hydrogel breaks. The force applied at the instant that the hydrogel broke was recorded as *F*. Additionally, the diameter of the hydrogel was measured, and the area *S* was calculated according to the formula $S=\pi r^2$. The force *F* and displacement at the time of specimen rupture were recorded, and the compressive strength was calculated according to the formula *P*=*F*/*S*.

Cytotoxicity Analysis The effect of the UV-polymerized hydrogel on the viability of L929 cells was studied by the CCK-8 method. The experiment was divided into three groups. The experiments were divided into three groups. The negative control group was the cell culture solution without hydrogel eluate, the positive control group was the cell culture solution without hydrogel eluate but with 5% dimethyl sulphoxide, and the hydrogel group was the cell culture solution with hydrogel eluate. Cells in the logarithmic phase of growth were collected, and cell suspensions at a density of 5×10^6/mL were added to 96-well culture plates. The culture plates were incubated in a 37°C incubator. After cell attachment, the culture medium was discarded, and 100 μL of the UV-polymerized hydrogel solution was added to the 96-well culture plate. The cells were incubated for 24, 48, or 72h in a 37°C constant temperature incubator with 5% CO_2. Next, 100 μL of culture medium containing 10% CCK-8 reagent was added to each well. After further cultivation for 24h, the absorbance values (OD values) of each well at a wavelength of 450 nm were measured using a microplate reader, and the cell viability was calculated as follows: cell viability (%)=[OD (drug added)–OD (blank)]/[OD (drug free)–OD (blank)]×100% where OD (drug added) is the absorbance value of the wells containing the hydrogel solution, OD (drug free) is the absorbance value of the wells without hydrogel solution, and OD (blank) is the absorbance value of the wells without cells.

Hemolysis Test The 3 mL of healthy rabbit blood was collected, centrifuged (1500 rpm, 15min), and rinsed gently 3 times with normal saline. The experiments were divided into three groups. The negative control group samples contained 1.1 mL of physiological saline and 100 μL of diluted red blood solution, and the positive control group samples contained 1.1 mL of deionized water and 100 μL of diluted red blood cell solution, and the hydrogel group samples contained 1 mL of normal saline, 100 μL of diluted red blood solution and 100 μL of hydrogel eluate. After 1h of incubation, the supernatants of all the samples were collected by centrifugation (1500 rpm, 15min), and 100 μL of each supernatant was placed in a 96-well plate. Finally, the OD of each sample was measured at 572 nm with a microplate reader and the hemolysis rate was calculated as [OD (hydrogel group)–OD (negative group)]/[OD (positive group)–OD (negative group)]×100%.

Apoptosis Detection The experiments were divided into three groups. The negative control group was the cell culture solution without hydrogel eluate, the positive control group was the cell culture solution without hydrogel eluate but with 5% dimethyl sulphoxide, and the hydrogel group was the cell culture solution with hydrogel eluate. L929 cells were inoculated into a 6-well plate and incubated in a constant temperature incubator for 24h. After discarding the culture medium, the above three groups of cell culture solutions with different treatments were added to the cells, and the culture was continued for 24, 48, or 72h. The cells were digested with trypsin without ethylene diamine tetraacetic acid and centrifuged, then the supernatant was discarded, and the cells were washed twice with phosphate buffer saline. The L929 cells were collected and resuspended in 1× binding buffer, then 10 μL of Annexin V-FITC and 5 μL of propidium iodide were added to the cells in the dark. After mixing, the cells were incubated at room temperature for 15min. Flow cytometry was used to determine the percentage of apoptotic cells in each group.

Animal Experiments Healthy one month old New Zealand white rabbits weighing approximately 500 g acquired from the Animal Center of Nanchang University were used for the *in vivo* experiments. To study the effect of hydrogel implantation into the orbit on the orbital development of young rabbits, the young rabbits (*n*=12) were randomly divided into three groups: the normal group (*n*=4), enucleation group (*n*=4), and enucleation+hydrogel implantation group (*n*=4).

Surgical Procedure The operation began after the young rabbit satisfied the effects of general anesthesia

[ketamine (35 mg/kg) and xylazine (5 mg/kg) administered intramuscularly]. The left eye of each rabbit was selected for surgery. After the young rabbits were fixed on the operating table, the conjunctival sac was washed with 0.9% sodium chloride and disinfected with iodophor. An eyelid opener was used to open the eyelid, and subconjunctival injection of lidocaine hydrochloride was used for local anesthesia. The bulbar conjunctiva was cut along the corneal margin in a circular manner. The extraocular muscles were removed, and the fascia and sclera were separated until the equatorial part of the eyeball was reached. The upper and lower eyelids were gently compressed so that the eyeball protruded outward. The optic nerve was quickly severed by applying hemostatic forceps for a few seconds, and the eyeball was removed. The eye socket was filled with sterile gauze for compression and to stop the bleeding. After removing the eyeball, in the enucleation group, the fascia and bulbar conjunctiva were directly sutured layer by layer, while in the enucleation+hydrogel implantation group, the sterile dry hydrogel (a cylinder with a diameter of 9 mm, a height of 3 mm, and a volume of 190.85 mm^3) was implanted into the orbit after enucleation, and then the fascia and bulbar conjunctiva layer were sutured layer by layer. The operated eyes were given levofloxacin eye drops, tobramycin dexamethasone eye ointment, and cephalosporins were given systemically to prevent infection.

Clinical Evaluations The overall and local conditions of the rabbits, the occurrence of systemic reactions such as breathing difficulty, decreased movement, diarrhea, abdominal irritation, and weight loss, were assessed. Moreover, assessments regarding redness and swelling in the operative eye, healing of the conjunctival incision, displacement, exposure, and prolapse of the hydrogel and other local conditions, were conducted. The healing status of the incision was evaluated and classified as follows: Grade A healing indicates good wound healing and no other adverse reactions; Grade B healing indicates the occurrence of inflammatory reactions such as redness, swelling, induration, or incision rupture at the incision site; Grade C healing indicates incision suppuration that required removal of the intraorbital implants.

Eye B Ultrasound and Magnetic Resonance Imaging Examinations In the three groups of young rabbits, an eye B ultrasound diagnostic apparatus (ODM-2100, MEDA, China) was used to observe changes in the orbit and shape of the hydrogel 1d and 4wk after surgery. The parameter settings for eye ultrasound were as follows: a digital high-precision motor-driven probe was used, the ultrasound frequency was 10 MHz, and the fan-shaped scanning method was applied. To clearly observe the changes in the hydrogel after implantation into the orbit, the three groups of young rabbits were subjected to magnetic resonance imaging (MRI; 3.0T Signa HDxt, GE, USA) tests 4wk after surgery. The young rabbits were placed in the supine position on the examination table with head pads placed on both sides of their heads to fix the head position, and the orbit was scanned.

Computed Tomography Examinations and Orbital Volume Measurements The following parameters were set when using a 128-layer spiral computed tomography (CT) machine (Definition AS, SIEMENS, Germany): voltage, 120 kV; current, 45 mA; time, 1s; acquisition layer thickness, 0.6 mm; layer spacing, 0.8 mm; window position, 40 Hu; and window width, 350 Hu. Images with a matrix of 512×512 were generated, and the scanning range included the entire skull. The scanned image was imported into the built-in image processing module for standardization before being transferred to the volume measurement module for automated measurements using a limited threshold (set to 160 HU to distinguish bony boundaries) combined with manual edge drawing tools to measure the orbital volume of the young rabbits. The optic nerve canal was not within the delineated range. Each operation was checked and measured by the same technician. The orbital volume of the young rabbits was measured before surgery and 4wk after surgery.

Organizational Examinations The young rabbits in the three groups were anesthetized and subsequently euthanized with an overdose of intravenous pentobarbital 4wk after surgery. The conjunctival fascia, liver, gallbladder, pancreas, spleen, kidney, and heart tissue were collected separately. All specimens were fixed in 10% paraformaldehyde, dehydrated in gradient alcohol, and then placed in xylene to make them transparent. The samples were then immersed in melted paraffin to embed the tissue. The embedded wax blocks were cut into slices with a thickness of 4 μm in sequence with a paraffin slicer. After baking, xylene was used for dewaxing, gradient alcohol was used to remove the xylene, and the sections were stained with hematoxylin and eosin (H&E), dehydrated and cleared before being sealed with neutral resin.

Statistical Analysis The data were analyzed using SPSS 25.0 software (USA) for statistical analysis and are expressed as the mean value±standard deviation. One-way analysis of variance followed by a post hoc Student-Newman-Keuls (SNK) test was used for comparisons of three or more groups. A value of $P<0.05$ was considered to indicate statistical significance.

RESULTS

Characterization of the UV-Polymerized Hydrogel Images of the UV-polymerized hydrogel as observed by the naked eye are shown in Figure 1A–1C. The dry hydrogel was yellowish in color with a smooth and flat surface, good light transmittance and a certain hardness, and had a diameter of approximately 9 mm (Figure 1A). After absorbing water and becoming completely swollen, the hydrogel appeared

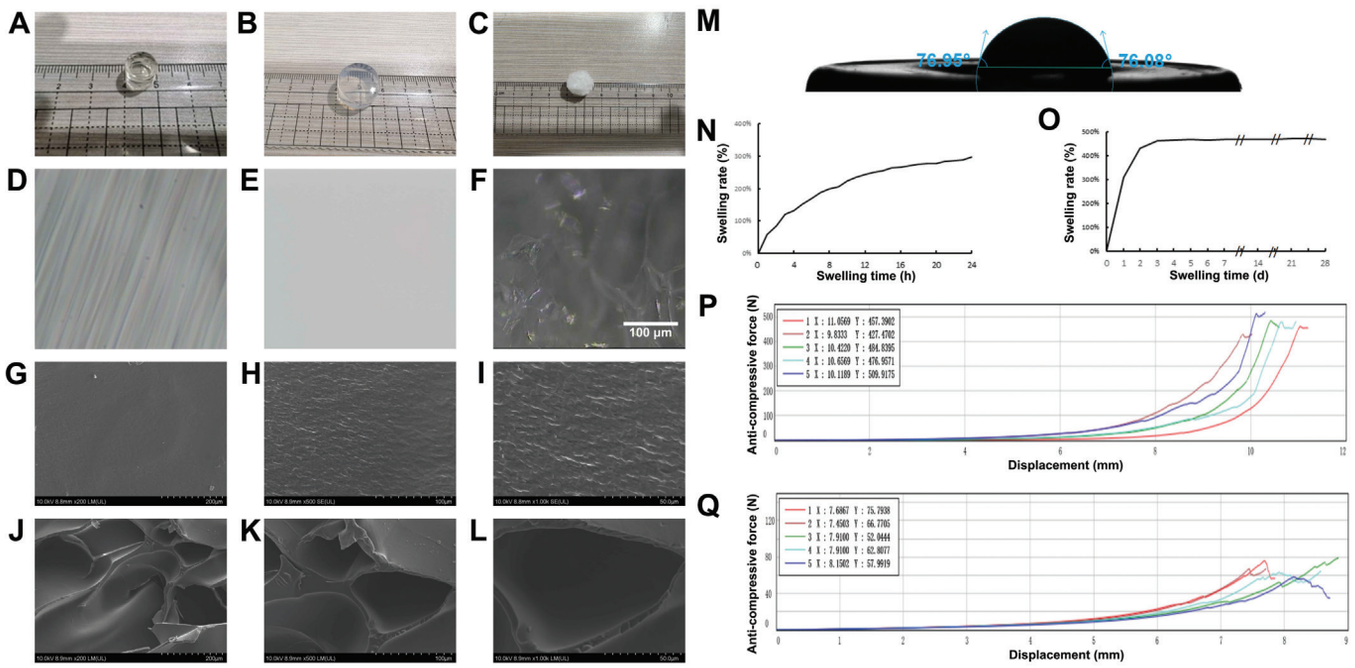

Figure 1 Characterization of the UV-polymerized hydrogel Naked-eye observations of the dry hydrogel (A), the swollen hydrogel that had fully absorbed water (B), and the vacuum freeze-dried hydrogel (C). Optical microscopy images of the dry hydrogel (D), the hydrogel that had fully absorbed water and swollen (E), and the vacuum freeze-dried hydrogel (F). Electron microscopy images of the dry hydrogel at 200× (G), 500× (H), and 1000× (I) magnification. Electron microscopy images of the vacuum freeze-dried hydrogel at 200× (J), 500× (K), and 1000× (L) magnification. Contact angle of the dry hydrogel (M). Swelling kinetics curves of the hydrogel after 1d (N) and 4wk (O). Anti-compressive forces and displacement curves of the hydrogels in the 1d (P) and 4wk (Q) water swelling groups. UV: Ultraviolet.

colorless, transparent, soft and flexible, with a diameter of approximately 16 mm (Figure 1B). The vacuum freeze-dried hydrogel was milky white, looked like cotton candy, and had slightly hardened with an uneven surface (Figure 1C). Optical microscopy images of the hydrogels are shown in Figure 1D–1F, where the dry hydrogels contained ribbon-like fibers (Figure 1D). After absorbing water and becoming completely swollen, the hydrogel became transparent (Figure 1E). After vacuum freeze drying, the hydrogel presented a three-dimensional network structure with visible pores (Figure 1F). The electron microscopy images of the dry hydrogel at 200×, 500×, and 1000× magnification are shown in Figure 1G–1I, which reveal that overall, the hydrogel had a complete, uniform and dense fiber network structure. Electron microscopy images of the vacuum freeze-dried hydrogel at 200×, 500×, and 1000× magnifications are shown in Figure 1J–1L. The freeze-dried hydrogel had a three-dimensional network structure in which evenly distributed pore-like gaps were observed and a diameter of approximately 130 μm.

Water contact angle of the dry hydrogels was measured to evaluate the hydrophilicity of the synthesized UV-polymerized hydrogels. The contact angle is an important indicator when examining the wettability of a liquid on a material surface. In this study, the water contact angle of the UV-polymerized hydrogel was 76.84°±1.52°, which indicates that it is hydrophilic (Figure 1M).

A hydrogel with a moderate swelling rate can promote orbital bone development and expand periorbital soft tissue. The average initial weight of the hydrogel in the one-day water absorption swelling group was 0.22±0.04 g, and the average weight increased to 0.88±0.16 g after one day of swelling. Thus, the swelling rate was 297.62%±11.91%, indicating that the hydrogel could absorb approximately 3 times its dry average weight of water after one day. The kinetics curve of the UV-polymerized hydrogel that had swelled for one day is shown in Figure 1N. The average initial weight of the hydrogel in the 4wk water absorption swelling group was 0.36±0.03 g, and the average weight increased 2.01±0.20 g and after 4d, giving a swelling rate of 464.73%±15.91% and essentially reaching equilibrium. After 28d, the average weight of the hydrogel was 2.02±0.19 g with a swelling rate of 467.81%±12.84%; implying that the hydrogel could absorb approximately 4.5 times its dry average weight of water after 28d. The kinetics curve of the UV-polymerized hydrogel that had swelled for 4wk is shown in Figure 1O.

The important indices of mechanical properties for swollen hydrogel include the anti-compression resistance, robustness to withstand breaking force, ease of being removed. The UV-polymerized hydrogel was allowed to expand for 1d and 4wk to evaluate its anti-compression resistance. The anti-compressive force and displacement curves of the 1d and 4wk are shown in Figure 1P–1Q. The breaking forces of

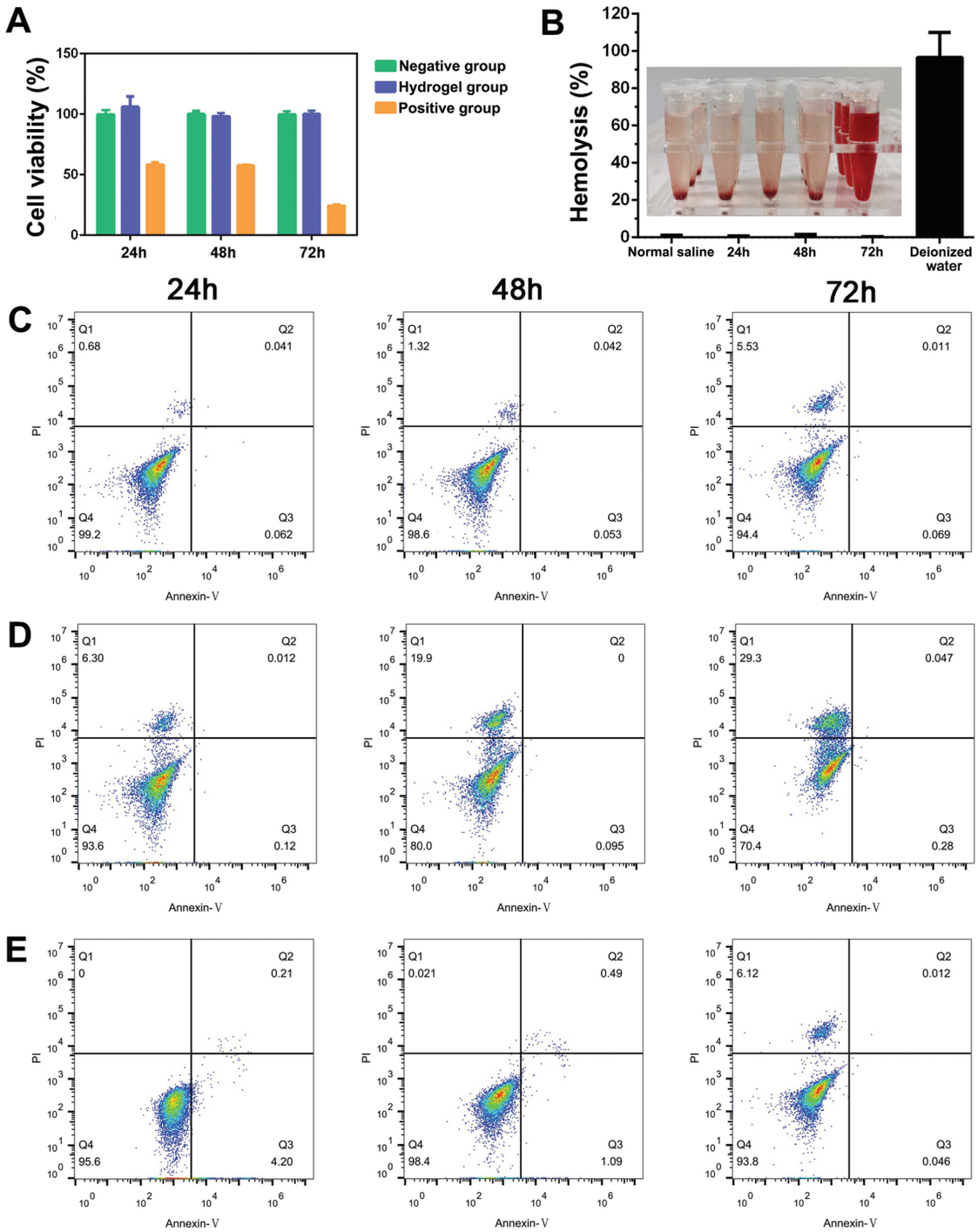

Figure 2 Biological properties of the UV-polymerized hydrogel eluate compared with negative and positive controls A: Viability of L929 cells for different durations. B: Hemolytic effect of normal saline group, hydrogel eluate cultured for 24, 48, 72h and deionized water group. C–E: Apoptosis in negative control group (C), positive control group (D), and hydrogel group (E) at different times. UV: Ultraviolet.

the hydrogels in the 1d and 4wk were 471.32±30.91 N and 63.08±8.99 N, respectively, and the anti-compressive strengths were 2.69±0.06 MPa and 0.30±0.03 MPa, respectively. These mechanical properties of hydrogels are desired for orbital implantation.

***In vitro* Biocompatibility Experiments** The CCK-8 method was used to determine the viability of L929 cells cultured with the UV-polymerized hydrogel eluate for different durations, as shown in Figure 2A. The relative viabilities of L929 cells cultured with the UV-polymerized hydrogel eluate for 24, 48, and 72h were all greater than 90% with no significant difference from that of the negative control group. These data indicated that the cells grew well with the hydrogel eluate and suggested that the cytotoxicity of the UV-polymerized hydrogel was low.

Additionally, the *in vitro* hemolysis of the UV-polymerized hydrogel eluate was evaluated after different durations with red blood cell cultures, as shown in Figure 2B. When the

UV-polymerized hydrogel eluate and red blood cells were cocultured for 24, 48 or 72h, no obvious hemolysis was observed.

The results of cell apoptosis analysis by flow cytometry were shown in Figure 2C–2E. L929 cells were cultured for 24, 48 and 72h with the UV-polymerized hydrogel eluate. There was no significant difference in the percentage of apoptotic cells between the control group and the hydrogel groups. For example, when L929 cells were treated with hydrogel eluate for 24h, the percentages of apoptotic cells in the negative control group, hydrogel group, and positive control group were 0.58%±0.82%, 1.94%±1.82%, and 3.97%±1.26%, respectively, and there were no significant differences between or within the groups. However, with the extension of culture time, there was still no statistical difference between the hydrogel group and the negative control group (P>0.05), but there were statistical differences with the positive control group (P<0.05).

Animal Studies

General conditions After surgery, none of the young rabbits in the three groups showed any significant systemic reactions, such as breathing difficulty, decreased movement, diarrhea, abdominal irritation, loss of appetite, or weight loss. The conjunctival incisions in the operative eyes healed well, and no local issues, such as displacement, exposure, or prolapse of the hydrogel, were observed, and Grade A healing was ascribed.

Eye ultrasound and MRI examinations The ultrasound results of the young rabbits 1d and 4wk after surgery are shown in Figure 3A–3B. As demonstrated in Figure 3A, in the normal control group, eye tissue was detected in the orbit along with curved and smooth eyeball walls and a strongly echogenic posterior capsule of the lens, which appeared with an arc shape. On the 1st day after enucleation, ultrasound examinations of the young rabbits revealed no palpable eye tissue in the orbit, and the orbital wall was curved and smooth. Moreover, scattered medium- to high-density shadows were visible in the orbit, suggesting the possibility of bleeding. One day after enucleation and hydrogel implantation, B ultrasound revealed that there was no eyeball tissue in the eye orbit, although dense dot-like medium–strong echoes were observed, the front and rear interfaces of the hydrogel were visible, and the hydrogel interior presented a low echo area. The MRI results of 4wk after surgery are shown in Figure 3C–3D. In the enucleation+hydrogel implantation group, clear and complete implants were observed in the orbits of the young rabbits with clear boundaries but no obvious inflammatory or necrotic tissue.

CT examinations and orbital volume measurements Figure 3E shows CT images of the three groups of young rabbits acquired 1d after surgery. The CT scans of the normal control group showed symmetrical and intact eyeballs on both sides. However, the postoperative CT scans after enucleation revealed orbital collapse but no ocular structure. In the enucleation+hydrogel implantation group, shadows with different densities were observed in the orbit, and hydrogel images were noted in CT. Figure 3F shows three-dimensional reconstruction images of the three groups of young rabbits in the colon shadowing mode taken 1d after surgery. The normal control group showed symmetrical and full bilateral orbits. In the enucleation group, orbital collapse was observed, but not an eyeball structure. In the enucleation+hydrogel implantation group, round hydrogels were seen in the orbit. The orbital volumes of the young rabbits in the normal group, enucleation group and enucleation+hydrogel implantation group were 2.60±0.06, 1.84±0.07, and 2.44±0.07 cm^3, respectively, at the time of 4wk after surgery. Compared with the enucleation group, the orbital volumes of the young rabbits in the enucleation+hydrogel implantation group was significantly increased (P<0.001). These results indicated that hydrogel implantation could significantly increase the orbital volume after enucleation.

Biosafety *in vivo* Figure 4 shows the H&E staining results of the conjunctival fascia, liver, gallbladder, pancreas, spleen, kidney, and heart tissues from the three groups of young rabbits at the time of 4wk after surgery. There were no significant abnormalities in the liver, gallbladder, pancreas, spleen, kidney, or heart tissues of these groups.

DISCUSSION

In this study, a new medical photo-polymerized hydrogel was synthesized by using monomers MMA and NVP, crosslinking agent AMA and EDGM, and initiator Irgacure 2959 under UV irradiation. The hydrogel had a three-dimensional network structure and good hydrophilicity, swelling and mechanical properties. The physical, chemical, and biological properties of the hydrogel were characterized, and its safety and effectiveness in ocular tissue expansion were preliminarily explored. The *in vitro* biocompatibility test showed that the UV-polymerized hydrogel did not affect the viability of L929 cells, did not cause red blood cell hemolysis, and did not increase apoptosis, indicating that the UV-polymerized hydrogel was biologically safe. B ultrasound, CT, MRI, and other imaging examinations of the eyes suggested that implantation of the hydrogel into the orbit stimulates the development of orbital bone in young rabbits and can prevent orbital hypoplasia after enucleation. The above results preliminarily suggest that this hydrogel is biologically safe and effective for tissue expansion.

Enucleation at an early age without an orbital implant may cause orbital bone dysplasia and facial asymmetry. As shown in this study, without an implant, the orbital volumes decreased from 2.60±0.06 cm^3 in the normal group to 1.84±0.07 cm^3 in

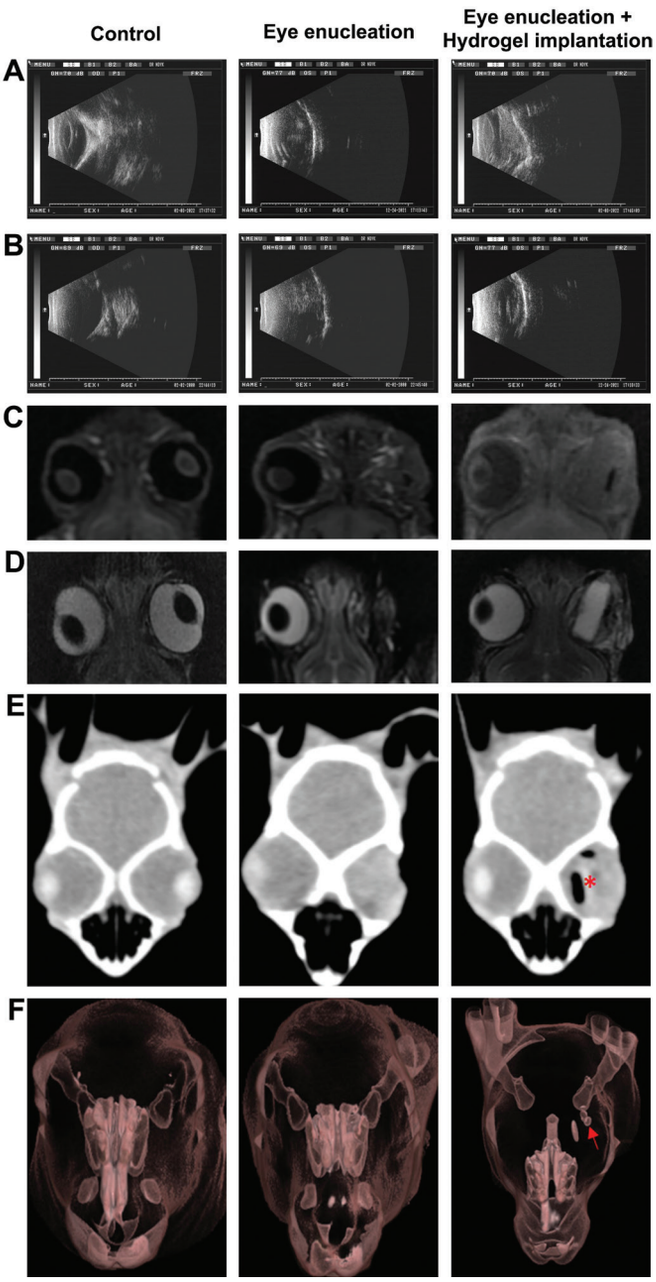

Figure 3 Imaging evaluations A, B: Ultrasound results of the three groups of young rabbits at the time of 1d (A) and 4wk (B) after surgery; C, D: MRI results of the young rabbits at the time of 4wk after surgery; E: CT images of young rabbits taken at the time of 1d after surgery; F: Three-dimensional reconstruction images of the young rabbits in colon shadow mode taken at the time of 1d after surgery. MRI: Magnetic resonance imaging; CT: Computed tomography.

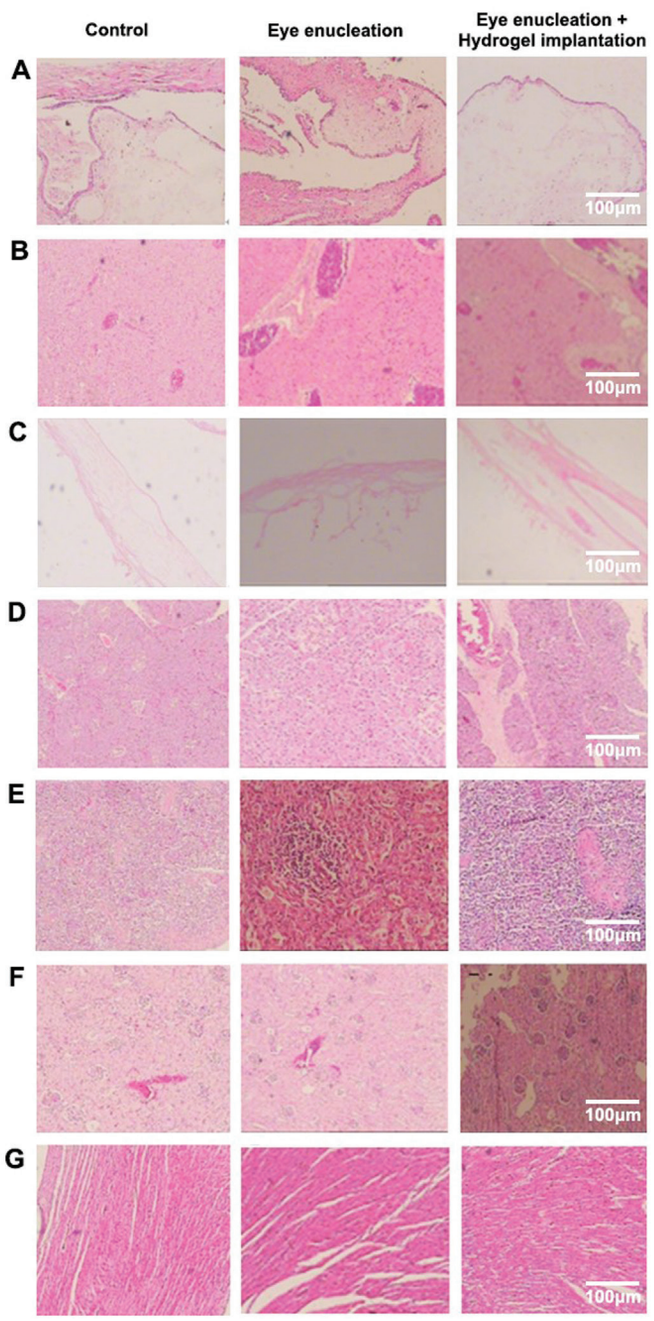

Figure 4 Biosafety *in vivo* H&E staining of conjunctival fascia (A), liver (B), gallbladder (C), pancreas (D), spleen (E), kidney (F), and heart (G) tissues from young rabbits at the time of 4wk after surgery. H&E: Hematoxylin and eosin.

the enucleation; in contrast, the orbital volume was largely maintained in the enucleation+hydrogel implantation group. The results suggest that an orbital implant after enucleation is critical for maintaining the orbital volume. Besides, ultrasound, CT, and MRI imaging examinations also illustrate the importance of hydrogel implantation into the orbit in orbital bone development in young rabbits and can prevent orbital hypoplasia after enucleation.

Currently, hydrogels have many applications in the treatment of ophthalmic diseases. Stimulus-responsive hydrogels can prolong drug retention in the eye and improve ocular bioavailability[36]. After ocular injury, treatment with hydrogel eye pads containing amniotic membrane extract may prevent rabbit eyelid adhesion[37]. Light-curable and tunable hydrogels can be used for *in situ* suture-free corneal repair[38]. Moreover, hydrogel dressing can improve the tear film stability of neurotrophic keratitis rats and promote the repair of damaged epithelial cells[39]. Hydrogel plugs generated *via* photo crosslinking can completely block lacrimal passage and greatly improve dry eye indices[40]. Hydrogel has important application

in stimulating orbital development, for instance, hydrogel implants can successfully enlarge the size of conjunctival sac and orbit in patients with congenital microphthalmia[41-43]. In our study, we presented an expandable polymer hydrogel material as the orbital filler to stimulate the development of orbital bone. The characteristics of the hydrophilic self-expanding hydrogel include its presetting of the water content, predictable swelling rate, ability to be wrapped after implantation, and low irritation to surrounding tissues.

In summary, UV curing was first introduced into a hydrogel formulation system, providing a new approach to the synthesis of medical hydrogels. The formulation, process, and synthesis route of this UV-polymerized hydrogel were independently developed, and the obtained hydrogel can meet the performance requirements after implantation into the orbit. The results presented here are expected to lead to the development of innovative biomaterials that promote the development of orbital tissue.

ACKNOWLEDGEMENTS

Foundations: Supported by the Science and Technology Plan Project of Jiangxi Province Health Commission (No.202210087; No.202310660; No.202610983); National Natural Science Foundation of China (No.52073136); Elite Talent Development Program of Nanchang First Hospital (No.202501004).

Conflicts of Interest: Zhang FB, None; **Chang YL,** None; **Tao XZ,** None; **Liu F,** None; **Liu CM,** None; **Hu HJ,** None; **Fang N,** None.

REFERENCES

1 Forer S, Ben Simon GJ, *et al*. Orbital development in children with retinoblastoma: an imaging-based study. *Semin Ophthalmol* 2024;39(5):369-375.

2 Wang N, Ke F, Li J, *et al*. Long-term observation of orbital development in patients with retinoblastoma following unilateral enucleation. *Cancer Med* 2025;14(19):e71282.

3 Furuta M. Measurement of orbital volume by computed tomography: especially on the growth of the orbit. *Jpn J Ophthalmol* 2001;45(6): 600-606.

4 Bentley RP, Sgouros S, Natarajan K, *et al*. Normal changes in orbital volume during childhood. *J Neurosurg* 2002;96(4):742-746.

5 Sigron GR, Britschgi CL, Gahl B, *et al*. Insights into orbital symmetry: a comprehensive retrospective study of 372 computed tomography scans. *J Clin Med* 2024;13(4):1041.

6 Fountain TR, Goldberger S, Murphree AL. Orbital development after enucleation in early childhood. *Ophthalmic Plast Reconstr Surg* 1999;15(1):32-36.

7 Wladis EJ, Aakalu VK, Sobel RK, *et al*. Orbital implants in enucleation surgery a report by the American academy of ophthalmology. *Ophthalmology* 2018;125(2):311-317.

8 Dasgupta D, Das K, Singh R. Rehabilitation of an ocular defect with intraorbital implant and custom-made prosthesis using digital photography and gridded spectacle. *J Indian Prosthodont Soc* 2019;19(3):266.

9 Ke F, Li J, Wang N, *et al*. Clinical characterization and long-term postoperative outcomes of retinoblastoma patients receiving enucleation and primary orbital implantation in early infancy: an observational study. *BMC Ophthalmol* 2024;24(1):360.

10 Wu WQ, Luo H, Wu D, *et al*. Biological activity of a vascular endothelial cell-hydroxyapatite orbital implant complex: an experimental study. *Exp Ther Med* 2022;23(3):227.

11 Han LS, Keillor RB, Weatherhead RG. Case series of shrinking hydroxyapatite orbital implants. *Br J Ophthalmol* 2021;105(10): 1338-1340.

12 Ding X, Su D, Cao Y, *et al*. Assessment of intraorbital hydroxyapatite implant exposure beyond 10 years of implantation. *Graefes Arch Clin Exp Ophthalmol* 2025;263(7):2025-2032.

13 Lin HY, Liao SL. Orbital development in survivors of retinoblastoma treated by enucleation with hydroxyapatite implant. *Br J Ophthalmol* 2011;95(5):630-633.

14 Chyzy A, Plonska-Brzezinska ME. Hydrogel properties and their impact on regenerative medicine and tissue engineering. *Molecules* 2020;25(24):5795.

15 Wang CG, Surat'man NEB, Chang JJ, *et al*. Polyelectrolyte hydrogels for tissue engineering and regenerative medicine. *Chem* 2022;17(18):e202200604.

16 Syed Mohamed SMD, Welsh GI, Roy I. Renal tissue engineering for regenerative medicine using polymers and hydrogels. *Biomater Sci* 2023;11(17):5706-5726.

17 Kuang ZH, Dai M. Application of graphene oxide-based hydrogels in bone tissue engineering. *ACS Biomater Sci Eng* 2022;8(7): 2849-2857.

18 Chen WX, Ming Y, Wang M, *et al*. Nanocomposite hydrogels in regenerative medicine: applications and challenges. *Macromol Rapid Commun* 2023;44(15):2300128.

19 Zhang Z, He CL, Chen XS. Designing hydrogels for immunomodulation in cancer therapy and regenerative medicine. *Adv Mater* 2024;36(4):2308894.

20 Lu LY, Yuan SL, Wang J, *et al*. The formation mechanism of hydrogels. *Curr Stem Cell Res Ther* 2018;13(7):490-496.

21 Zhang D, Li ZM, Yang L, *et al*. Architecturally designed sequential-release hydrogels. *Biomaterials* 2023;303:122388.

22 Morozova SM, Gevorkian A, Kumacheva E. Design, characterization and applications of nanocolloidal hydrogels. *Chem Soc Rev* 2023;52(15):5317-5339.

23 Bai RB, Yang JW, Morelle XP, *et al*. Flaw-insensitive hydrogels under static and cyclic loads. *Macromol Rapid Commun* 2019;40(8):1800883.

24 Wang L, Zhao W, Zhao YN, *et al*. Enzymatically-mineralized double-network hydrogels with ultrahigh mechanical strength, toughness, and stiffness. *Theranostics* 2023;13(2):673-684.

25 Zhu MR, Zhang H, Zhou QR, *et al*. Dynamic GelMA/DNA dual-network hydrogels promote woven bone organoid formation and enhance bone regeneration. *Adv Mater* 2025;37(24):2501254.

26 Kang JW, Li YP, Qin YT, *et al*. *In situ* deposition of drug and gene nanoparticles on a patterned supramolecular hydrogel to construct a directionally osteochondral plug. *Nano Micro Lett* 2023;16(1):18.

27 Haas S, Körner S, Zintel L, *et al*. Changing mechanical properties of photopolymerized, dityrosine-crosslinked protein-based hydrogels. *Front Bioeng Biotechnol* 2022;10:1006438.

28 Wang X, Li FQ, Liu X, *et al*. Applications and recent developments of hydrogels in ophthalmology. *ACS Biomater Sci Eng* 2023;9(11):5968-5984.

29 Batta-Mpouma J, Kandhola G, Sakon J, *et al*. Covalent crosslinking of colloidal cellulose nanocrystals for multifunctional nanostructured hydrogels with tunable physicochemical properties. *Biomacromolecules* 2022;23(10):4085-4096.

30 Shen KH, Yeh YY, Chiu TH, *et al*. Dual dynamic covalently crosslinked alginate hydrogels with tunable properties and multiple stimuli-responsiveness. *ACS Biomater Sci Eng* 2022;8(10):4249-4261.

31 Park S, Kim D, Ko SY, *et al*. Controlling uniformity of photopolymerized microscopic hydrogels. *Lab Chip* 2014;14(9):1551-1563.

32 Brown TE, Carberry BJ, Worrell BT, *et al*. Photopolymerized dynamic hydrogels with tunable viscoelastic properties through thioester exchange. *Biomaterials* 2018;178:496-503.

33 Nicol E. Photopolymerized porous hydrogels. *Biomacromolecules* 2021;22(4):1325-1345.

34 Censi R, Vermonden T, van Steenbergen MJ, *et al*. Photopolymerized thermosensitive hydrogels for tailorable diffusion-controlled protein delivery. *J Control Release* 2009;140(3):230-236.

35 Nelson BR, Kirkpatrick BE, Miksch CE, *et al*. Photoinduced Dithiolane Crosslinking for Multiresponsive Dynamic Hydrogels. *Adv Mater* 2024;36(43):e2211209.

36 Lin DQ, Lei L, Shi S, *et al*. Stimulus-responsive hydrogel for ophthalmic drug delivery. *Macromol Biosci* 2019;19(6):1900001.

37 Chen J, Wang MW, Xu JJ, *et al*. Gelatin methacryloyl hydrogel eye pad loaded with amniotic extract prevents symblepharon in rabbit eyes. *Eur Rev Med Pharmacol Sci* 2020;24(19):10134-10142.

38 Yazdanpanah G, Shen X, Nguyen T, *et al*. A light-curable and tunable extracellular matrix hydrogel for *in situ* suture-free corneal repair. *Adv Funct Mater* 2022;32(24):2113383.

39 Xia HQ, Song YF, *et al*. Hydrogel dressings on neurotrophic keratitis in an experimental animal model. *Int J Ophthalmol* 2024;17(8): 1396-1402.

40 Dai ML, Xu KJ, Xiao DC, *et al*. *In situ* forming hydrogel as a tracer and degradable lacrimal plug for dry eye treatment. *Adv Healthc Mater* 2022;11(19):2200678.

41 Hou ZJ, Yang Q, Chen T, *et al*. The use of self-inflating hydrogel expanders in pediatric patients with congenital microphthalmia in China. *J Am Assoc Pediatr Ophthalmol Strabismus* 2012;16(5):458-463.

42 Ma L, Hou ZJ, Zhang J, *et al*. Stepwise self-inflating hydrogel expansion for congenital anophthalmia and blind microphthalmia: Over 15 years' experience in China. *J Plast Reconstr Aesthetic Surg* 2024;90:40-46.

43 Alanazi RR, Schellini SA, Alhussain H, *et al*. Outcomes of the use of orbital hydrogel expanders in the management of congenital anophthalmia: CT-based orbital parameter analysis. *Orbit* 2022;41(6):691-699.